Atmos. Chem. Phys., 13, 3027–3044, 2013
www.atmos-chem-phys.net/13/3027/2013/
doi:10.5194/acp-13-3027-2013

Atmospheric Chemistry and Physics Open Access

Impact of the modal aerosol scheme GLOMAP-mode on aerosol forcing in the Hadley Centre Global Environmental Model

N. Bellouin[1,*], G. W. Mann[2,3], M. T. Woodhouse[3], C. Johnson[1], K. S. Carslaw[3], and M. Dalvi[1]

[1]Met Office Hadley Centre, Exeter, UK
[2]National Centre for Atmospheric Science, University of Leeds, Leeds, UK
[3]Institute for Climate and Atmospheric Science, School of Earth and Environment, University of Leeds, Leeds, UK
[*]now at: Department of Meteorology, University of Reading, Reading, UK

Correspondence to: N. Bellouin (n.bellouin@reading.ac.uk)

Received: 31 July 2012 – Published in Atmos. Chem. Phys. Discuss.: 21 August 2012
Revised: 4 February 2013 – Accepted: 4 March 2013 – Published: 15 March 2013

Abstract. The Hadley Centre Global Environmental Model (HadGEM) includes two aerosol schemes: the Coupled Large-scale Aerosol Simulator for Studies in Climate (CLASSIC), and the new Global Model of Aerosol Processes (GLOMAP-mode). GLOMAP-mode is a modal aerosol microphysics scheme that simulates not only aerosol mass but also aerosol number, represents internally-mixed particles, and includes aerosol microphysical processes such as nucleation. In this study, both schemes provide hindcast simulations of natural and anthropogenic aerosol species for the period 2000–2006. HadGEM simulations of the aerosol optical depth using GLOMAP-mode compare better than CLASSIC against a data-assimilated aerosol re-analysis and aerosol ground-based observations. Because of differences in wet deposition rates, GLOMAP-mode sulphate aerosol residence time is two days longer than CLASSIC sulphate aerosols, whereas black carbon residence time is much shorter. As a result, CLASSIC underestimates aerosol optical depths in continental regions of the Northern Hemisphere and likely overestimates absorption in remote regions. Aerosol direct and first indirect radiative forcings are computed from simulations of aerosols with emissions for the year 1850 and 2000. In 1850, GLOMAP-mode predicts lower aerosol optical depths and higher cloud droplet number concentrations than CLASSIC. Consequently, simulated clouds are much less susceptible to natural and anthropogenic aerosol changes when the microphysical scheme is used. In particular, the response of cloud condensation nuclei to an increase in dimethyl sulphide emissions becomes a factor of four smaller. The combined effect of different 1850 baselines, residence times, and abilities to affect cloud droplet number, leads to substantial differences in the aerosol forcings simulated by the two schemes. GLOMAP-mode finds a present-day direct aerosol forcing of $-0.49\,\mathrm{W\,m^{-2}}$ on a global average, 72 % stronger than the corresponding forcing from CLASSIC. This difference is compensated by changes in first indirect aerosol forcing: the forcing of $-1.17\,\mathrm{W\,m^{-2}}$ obtained with GLOMAP-mode is 20 % weaker than with CLASSIC. Results suggest that mass-based schemes such as CLASSIC lack the necessary sophistication to provide realistic input to aerosol-cloud interaction schemes. Furthermore, the importance of the 1850 baseline highlights how model skill in predicting present-day aerosol does not guarantee reliable forcing estimates. Those findings suggest that the more complex representation of aerosol processes in microphysical schemes improves the fidelity of simulated aerosol forcings.

1 Introduction

Within the Earth's climate system, atmospheric aerosols interact with solar and thermal radiation through scattering and absorption, processes termed as direct radiative effects. Aerosols also influence cloud microphysical properties, impacting cloud albedo and precipitation, and indirectly affecting radiative fluxes again (Forster et al., 2007). Aerosols also interact with biogeochemical cycles in the atmosphere and ocean, ice surfaces, and atmospheric chemistry (Carslaw et al., 2010). Those multiple interactions justify the inclusion

of both natural and anthropogenic aerosols in numerical models of the climate system. The radiative effects of anthropogenic aerosols are considered an external influence and are termed radiative forcings.

The quantification of aerosol radiative forcing involves knowledge of the horizontal, vertical, and temporal distributions of mass, number, chemical composition, state of mixture, size, and shape of the aerosols. In addition, environmental characteristics such as relative humidity, clouds, and the albedo of the underlying surface influence the magnitude and sign of aerosol forcing. Because aerosols are short-lived species in the troposphere, the parameters listed above vary greatly in space and time. Observations do not constrain well the multiple aspects of aerosol distributions. In numerical models, simulation of the aerosol life cycle is complicated by the large uncertainties surrounding natural and anthropogenic aerosol emission, transport, ageing, and removal processes. Consequently, aerosol forcing of climate is uncertain. Estimates for the direct forcing have been assessed at $-0.4 \pm 0.4\,\mathrm{W\,m^{-2}}$ (Forster et al., 2007). Observational estimates are typically stronger than modelled estimates, although agreement can be achieved when differences in sampling (Bellouin et al., 2008) and historical changes in aerosol absorption (Myhre, 2009) are taken into account. Indirect forcing estimates have been given the large 5–95 % range of -0.3 to $-1.8\,\mathrm{W\,m^{-2}}$ (Forster et al., 2007). Observational estimates tend to be weaker than modelled estimates (Quaas et al., 2009) for reasons that remain unclear and debated (Penner et al., 2011).

In numerical models, uncertainty and diversity affect all stages of aerosol representations, from aerosol sources to aerosol sinks. Schulz et al. (2006) showed by comparing nine simulations by international aerosol modelling groups that diversity in direct forcing estimates is due to differences in simulated aerosol residence time, dry mass extinction coefficient, chemical production from the gas phase, and vertical profile compared to clouds. All simulations shared the same emission datasets, thus factoring out this additional source of diversity. Lee et al. (2011) investigated the contributions to uncertainty in simulated concentrations of cloud condensation nuclei (CCN) by running ensembles of simulations of a global aerosol microphysics model. They found that, although emissions uncertainties explained most of the CCN uncertainty near to source regions, uncertainties in marine and remote regions were dominated by parametric uncertainty in aerosol processes.

Numerical aerosol representations have become more sophisticated over the last decade. First-generation aerosol schemes in climate models tend to transport only aerosol mass, deriving particle number concentrations using prescribed and uniform size distributions within several aerosol types. Simulating growth processes like condensation of low-volatility gases and aqueous sulphate production in these mass-based schemes is problematic since simulated particle number does not change proportionally with changes in aerosol mass. In contrast, two-moment sectional aerosol schemes (Adams and Seinfeld, 2002; Spracklen et al., 2005; Kokkola et al., 2008) simulate both mass and number in multiple size bins allowing the particle size distribution to evolve freely according to the model processes. However, the need to keep track of aerosol mass and composition in each size bin makes such schemes costly to run in a large-scale general circulation model. Two-moment modal schemes have been developed as a compromise: they also simulate both aerosol mass and number, but the aerosol size distribution is represented by a superposition of modes, typically assumed log-normal (Ghan et al., 2001; Easter et al., 2004; Stier et al., 2005; Liu et al., 2005; Lauer et al., 2005; Bauer et al., 2008; Pringle et al., 2010; Liu et al., 2012). The M7 scheme (Vignati et al., 2004) and the Global Model of Aerosol Processes modal scheme, GLOMAP-mode (Mann et al., 2010), define 7 modes, representing a nucleation mode, and soluble and insoluble modes for each of the Aitken, accumulation and coarse size ranges.

The Hadley Centre Global Environmental Model, HadGEM, has included various incarnations of the aerosol mass scheme CLASSIC (Coupled Large-scale Aerosol Simulator for Studies in Climate) since its first version, HadGEM1 (Martin et al., 2006). CLASSIC is used in the HadGEM2 family of models (Martin et al., 2011), including the Earth System version used for the Hadley Centre's contribution to the Climate Model Intercomparison Project phase 5 (CMIP5) database (Bellouin et al., 2011). In parallel, the two-moment modal scheme GLOMAP-mode (Mann et al., 2010) has been added to HadGEM as part of the United Kingdom Chemistry and Aerosol (UKCA) model, having first been developed in the chemistry-transport model TOMCAT (Chipperfield, 2006). The presence of the mass-based CLASSIC scheme and the microphysical GLOMAP-mode scheme within the same model framework provides the opportunity to investigate how aerosol forcing depends on the aerosol scheme itself, and whether older results are challenged by the new scheme. GLOMAP-mode is expected to better represent the physical mechanisms involved in aerosol-cloud interactions, while maintaining the quality of the simulation of aerosol optical depths and direct effects.

The paper is structured as follows. The next section highlights the relevant differences between the CLASSIC and GLOMAP-mode aerosol schemes. Section 3 describes the model simulations analysed, and summarises the main properties of the aerosols in those simulations. Section 4 quantifies the skill of each aerosol scheme at simulating total aerosol optical depths. Skill is measured by comparing against observations and data-assimilated modelling. Results on aerosol direct and indirect effects are presented in Sects. 5 and 6. Section 7 then discusses aerosol forcing in the two schemes. To conclude, consequences for aerosol forcing uncertainty and older modelling results are discussed.

2 Aerosol schemes

The aerosol mass scheme CLASSIC simulates eight aerosol species: ammonium sulphate, mineral dust, fossil-fuel black carbon, fossil-fuel organic carbon, biomass-burning, ammonium nitrate (which is not activated in this study), sea-salt, and secondary organic aerosols from biogenic emissions. For most species, aerosol mass is distributed across three model tracers associated with the Aitken, accumulation, and dissolved (or in-cloud) modes. Exceptions are mineral dust, which uses six size bins; nitrate, which does not have an Aitken mode; sea-salt, which is not transported but computed at each model time step depending on instantaneous near-surface wind speeds; and secondary organic aerosols, which are represented by a monthly-averaged climatology of mass-mixing ratios. CLASSIC uses 22 model tracers, including the tracers required for sulphur dioxide and ammonia. The eight CLASSIC aerosol species exert direct radiative effects, and indirect effects are exerted by all species except mineral dust and fossil-fuel black carbon. A detailed description of CLASSIC is available in the appendix of Bellouin et al. (2011).

In this study, the modal aerosol scheme GLOMAP-mode simulates the mass of four aerosol species: sulphate, black carbon, organic carbon, and sea-salt. The carbonaceous components have emissions sources from bio-fuel, fossil-fuel and biomass burning, with organic carbon also receiving a secondary source from the oxidation of monoterpenes. Mineral dust aerosols are not yet available within the modal framework as implemented in HadGEM, and CLASSIC bin-resolved mineral dust is used. The representation of nitrate aerosols remains in development. GLOMAP-mode also simulates the aerosol number in four soluble modes representing nucleation, Aitken, accumulation, and coarse-mode particles, and an insoluble mode for Aitken particles, as summarised in Table 1. For soluble modes, GLOMAP-mode also simulates the equilibrium water content of the aerosols. GLOMAP-mode uses 31 model tracers, including tracers for sulphur dioxide, secondary organic compounds, and CLASSIC mineral dust. All aerosol species exert direct and indirect radiative effects, except for CLASSIC mineral dust, which only exerts direct effects. A comprehensive description of GLOMAP-mode is given in Mann et al. (2010), and its implementation within the Hadley Centre general circulation model is described by Johnson et al. (2010).

Figure 1 summarises the two aerosol schemes and highlights the two key differences between them. Firstly, CLASSIC is a bulk model that treats aerosol mass according to emitted aerosol components. Aerosol number is diagnosed from aerosol mass. External mixture is assumed for aerosol interactions with radiation and when cloud droplet number concentrations are computed from aerosol distributions. In contrast, GLOMAP-mode represents aerosol microphysics. Aerosol components are internally mixed within each mode, although not all modes are expected to contain all components (Table 1). Those differences impact the calculation of aerosol optical properties, as described in Sect. 5. Secondly, GLOMAP-mode includes aerosol microphysical processes that CLASSIC does not. Of particular interest is the addition of a nucleation mode to simulate secondary particle formation via binary nucleation of sulphuric acid and water. Overall, GLOMAP-mode includes intra- and inter-modal coagulation, condensation of sulphuric acid and secondary organic compounds onto exiting particles, ageing of insoluble into soluble particles, mode merging when particle sizes exceed modal boundaries, and cloud processing (Mann et al., 2010). In both schemes, aerosol sulphate mass is produced via gas phase and aqueous oxidation of sulphur dioxide. GLOMAP-mode additionally includes a gas-phase sulphuric acid tracer, produced via in-air oxidation of sulphur dioxide, which determines nucleation and condensation rates on a shorter competition timestep as described in Spracklen et al. (2005) and Mann et al. (2010). For carbonaceous components, both schemes account for condensation of volatile organic compounds. CLASSIC simply increases the biomass-burning aerosol mass by 62 % upon ageing after an e-folding time of 6 h. The additional mass is added to the biomass-burning aerosol without being taken from another tracer. GLOMAP-mode has a more mechanistic representation and uses a gas-phase secondary organic compound tracer replenished by oxidation of monoterpene by ozone and the hydroxyl and nitrate radicals. Both schemes remove aerosols by dry and wet deposition, the latter for both convective and large-scale precipitation. Because CLASSIC uses so-called dissolved modes to independently represent the aerosols that are dissolved in cloud droplets (Jones et al., 2001), CLASSIC wet deposition is better linked to the modelled precipitation, and includes evaporation of precipitation. GLOMAP-mode includes both nucleation and impaction scavenging following the approaches used in the offline chemistry transport model framework as described by Mann et al. (2010). In the HadGEM implementation of GLOMAP-mode however, nucleation scavenging proceeds at a rate determined by the precipitation rates simulated by the atmosphere model, rather

Table 1. Solubility, size boundaries, and composition of the five modes in the GLOMAP-mode aerosol scheme. Components are sulphate (SU), black carbon (BC), organic carbon (OC) and sea-salt (SS). r is the geometric mean radius of the aerosol particles, including hygroscopic growth for soluble modes, in nm.

Mode	Soluble?	Size boundaries	Composition
Nucleation	Yes	$r < 5$	SU
Aitken	Yes	$5 < r < 50$	SU, BC, OC
Accumulation	Yes	$50 < r < 500$	SU, BC, OC, SS
Coarse	Yes	$r > 500$	SU, BC, OC, SS
Aitken	No	$5 < r < 50$	BC, OC

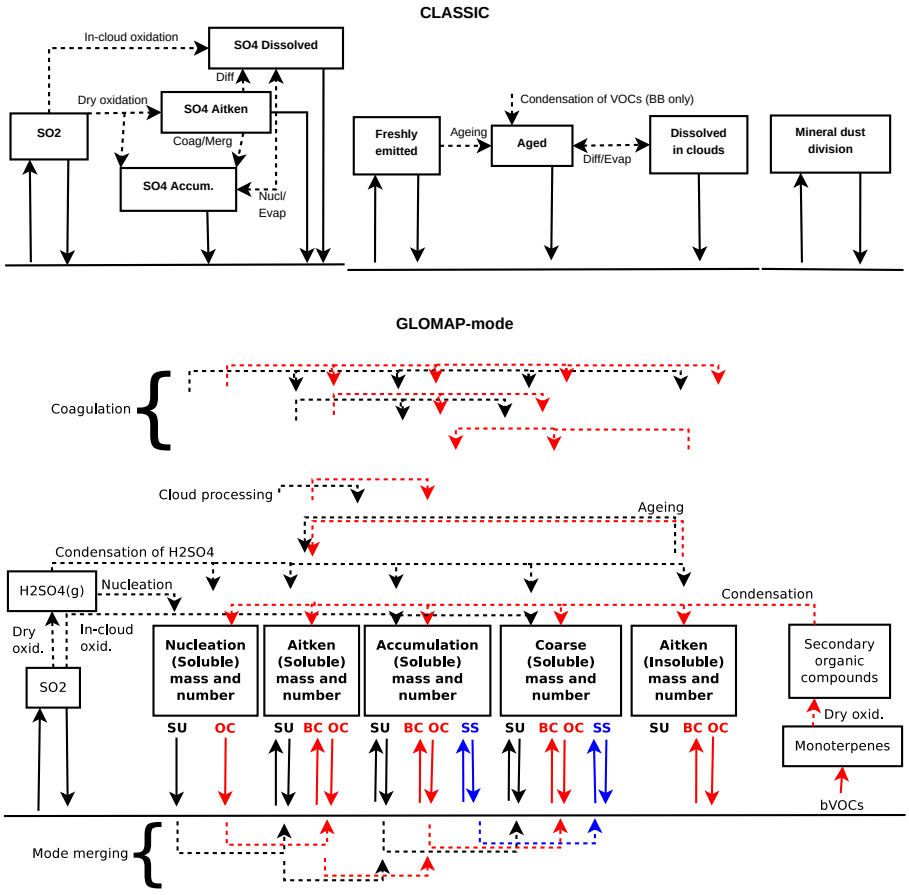

Fig. 1. Summary of CLASSIC (top) and GLOMAP-mode (bottom) aerosol schemes. CLASSIC represents the mass of the external mixture of sulphur cycle (left), carbonaceous (middle), and mineral dust aerosols (right). CLASSIC sea-salt and secondary organic aerosols are purely diagnostic and are not represented on those diagrams. GLOMAP-MODE simulates the mass and number of five aerosol modes where sulphate (SU, black), black and organic carbon (BC and OC, red), and sea-salt (SS, blue) aerosols are internally mixed. Solid arrows represent the total emission and deposition mass fluxes. Dashed arrows represent mass fluxes within each scheme.

than the constant timescale approach used in the offline transport model. Finally, note that CLASSIC sea-salt aerosols are diagnosed at each timesteps from near-surface wind speeds, and secondary organic aerosols are represented by monthly-means climatologies of mass-mixing ratios. They are therefore not transported tracers, and are not represented in Fig. 1.

3 HadGEM simulations

The two aerosol schemes are used in hindcast simulations of the period 2000–2006 with HadGEM. Aerosol emission datasets are those prepared for the AeroCom Hindcast experiments (Diehl et al., 2012). Baseline fossil-fuel and biofuel black and organic carbon emissions are taken from Bond et al. (2004) for the year 1996, and sulphur dioxide emissions are taken from the EDGAR v4.1 database for the year 2000, available at edgar.jrc.ec.europa.eu. Sectors included are residential, industry, power generation, and transport. Trends are then applied in 17 regions following Streets et al. (2004). Over Europe, a seasonal variation is applied to sulphur dioxide emissions such that 32.5 % of annual emissions occur in December-January-February, 25 % in March-April-May, 17.5 % in June-July-August, and 25 % in September-October-November. GLOMAP-mode emits 2.5 % of sulphur dioxide emissions as primary sulphate aerosol. Biomass-burning emissions are taken from the Global Fire Emissions Database (GFED) version 2 (van der Werf et al., 2004). Emissions from international shipping are taken from Eyring et al. (2005a,b).

For technical reasons, the two schemes in this study are run in slightly different versions of the HadGEM atmosphere model, both however nudged to the same ERA Interim 6-hourly temperature and wind fields (Telford et al., 2008), and using the same horizontal and vertical resolutions of 1.875° by 1.25° and 38 vertical levels with the model top at about 39 km. CLASSIC was run in the atmosphere-only version of the Earth System model HadGEM2-ES (Collins et al., 2011). GLOMAP-mode was run in a developmental version

of HadGEM3, the successor of HadGEM2. Differences between the models include changes in the scientific configuration of the boundary-layer and convection parameterisations, and the use of the PC2 prognostic cloud scheme (Wilson et al., 2008) in HadGEM3. Although those differences are expected to affect aerosol transport and removal processes, it has been checked by running CLASSIC in the same version of HadGEM3 that differences due to the host model are small compared to those discussed in the paper. It is also worth noting that in spite of aerosol radiative effects affecting model evolution differently in the two simulations, nudging ensures that synoptic atmosphere dynamics remain similar. Sulphur-cycle oxidants, the hydroxyl radical (OH), ozone (O_3), and hydrogen peroxide (H_2O_2), are supplied to CLASSIC by the UK Chemistry and Aerosol (UKCA) tropospheric chemistry scheme, which is summarised in the appendix of Bellouin et al. (2011). For GLOMAP-mode, sulphur dioxide and dimethyl sulphide are oxidised in the UKCA gas-phase chemical scheme, together with aqueous-phase oxidation of sulphur dioxide. There is a sulphuric acid tracer which is passed to GLOMAP-mode for aerosol nucleation and condensation processes. The aqueous phase sulphur dioxide oxidation rates are used for in-cloud aerosol processing. Mineral dust is simulated using the CLASSIC scheme in both CLASSIC and GLOMAP-mode simulations. However, due to different calibrations of the mineral dust emission scheme in HadGEM2 and HadGEM3, and different near-surface wind speeds, mineral dust size distributions and residence times differ in the two simulations. Manktelow et al. (2010) have shown that mineral dust has a small impact on the aerosol components that are evaluated in this study. CLASSIC nitrate is not activated in order to retain a close match between the aerosol species included in the two schemes.

Table 2 shows global, multi-annual averages of the key variables that characterise the CLASSIC and GLOMAP-mode simulations. In order to match the GLOMAP-mode list of species, mass and deposition rates of CLASSIC biomass-burning and fossil-fuel carbonaceous aerosols have been distributed into black and organic carbon, using a 5.4 % black carbon mass fraction for biomass-burning aerosols, as assumed in the refractive index of the aged mode. Note however that the black carbon fraction in biomass-burning emissions is different, at 11 % on a global, multi-annual average. Although Table 2 only gives the main mass fluxes, it has been checked for both aerosol schemes that emission and chemical production (where applicable) rates equal deposition and chemical destruction rates for all species within a few percent on a global, multi-annual average. For the sulphur cycle, the ratio of sulphate aerosol deposition to sulphur dioxide anthropogenic emission is smaller in GLOMAP-mode than in CLASSIC. This suggests that the rates of sulphur dioxide oxidation and sulphuric acid condensation into the aerosol phase are slower in GLOMAP-mode than in CLASSIC, which only represents oxidation processes. Indeed, GLOMAP-mode maintains 0.64 ± 0.03 Tg[S] as sulphur dioxide in the atmosphere over the simulated period, 1.6 times more than CLASSIC at 0.39 ± 0.02 Tg[S]. For carbonaceous aerosols, primary emissions are complemented by condensation of volatile organic compounds, leading to increases in deposition rates compared to primary emission rates. On a global, multi-annual average, organic carbon aerosol mass increases by a factor 1.5 in CLASSIC, 1.6 in GLOMAP-mode. Therefore, this aspect is in good agreement between the two schemes, in spite of the simple representation of volatile organic compound condensation in CLASSIC.

As explained above, CLASSIC mineral dust aerosols are quite different in the two simulations, with much larger mineral dust emissions in HadGEM3 than HadGEM2. Other notable differences between the two schemes are the residence times of sulphate and black carbon aerosols. Sulphate resides in the atmosphere two days longer in GLOMAP-mode than in CLASSIC because parameterisations of wet deposition differ between the two schemes, as discussed in the last paragraph of Sect. 2 above, and the parameterisation used by GLOMAP-mode ends up yielding smaller deposition rates of sulphate aerosols. To a smaller extent, the longer residence time of sulphur dioxide is also likely to allow transport to regions where, once oxidation has taken place, precipitation and wet removal of sulphate aerosols are smaller. In contrast, black carbon residence time is longer in CLASSIC than in GLOMAP-mode by 10 days. This is a known limitation of CLASSIC, where the hydrophobic nature of aged fossil-fuel black carbon aerosols prevents efficient wet removal (Bellouin et al., 2011). Finally, although sea-salt burden in CLASSIC is much larger than in GLOMAP-mode, this is of little consequence for sea-salt radiative effects. The CLASSIC sea-salt diagnostic scheme puts a large fraction of the total mass in the jet mode, which is made of coarse particles. The jet mode is therefore optically inefficient for the direct effect, and provides little aerosol number for the parameterisation of the first indirect effect used in this study, described in Sect. 6.

4 Aerosol optical depth

CLASSIC assumes external mixing of aerosol components, and therefore allows the computation of aerosol optical depths (AODs) for each component. In contrast, GLOMAP-mode AODs are computed for each mode, as internal mixing within each mode prevents the identification of the contribution by an individual species. Over the 2000–2006 period, the total global-averaged AOD at 0.55 µm is 0.114 ± 0.002 in CLASSIC, and 0.116 ± 0.003 in GLOMAP-mode. Here and in the rest of the paper, standard deviations measure the inter-annual variability over the simulated period. CLASSIC sea-salt and sulphate are the main contributors to the total AOD, at 0.052 (46 %) and 0.027 (24 %), respectively. In GLOMAP-mode, the main contributor is the accumulation-soluble mode

Table 2. Key parameters of simulated aerosol distributions using CLASSIC and GLOMAP-modes aerosol schemes in hindcast simulations of 2000–2006. Sulphur-cycle emissions are for sulphur dioxide, but remaining variables are for sulphate aerosols. For deposition rates, numbers in brackets give the percentage due to dry deposition. CLASSIC sea-salt aerosols are not transported tracers and are not emitted nor deposited. Standard deviations measure the variability over the 2000–2006 period.

	CLASSIC	GLOMAP-mode	CLASSIC	GLOMAP-mode
	Sulphur cycle [S]		Black carbon [C]	
Emissions ($Tg\,yr^{-1}$)	79.5 ± 3.2	79.5 ± 3.2	7.6 ± 0.3	7.6 ± 0.4
Burden (Tg)	0.54 ± 0.02	0.66 ± 0.05	0.30 ± 0.01	0.10 ± 0.01
Deposition ($Tg\,yr^{-1}$)	64.7 ± 2.0 (11 %)	46.5 ± 1.6 (6 %)	7.1 ± 0.4 (18 %)	7.6 ± 0.4 (34 %)
Residence time (days)	3.0 ± 0.1	5.1 ± 0.2	15.0 ± 0.4	5.0 ± 0.1
	Organic carbon [C]		Sea-salt	
Emissions ($Tg\,yr^{-1}$)	29.7 ± 1.8	33.3 ± 2.0		3302.1 ± 41.5
Burden (Tg)	0.91 ± 0.04	0.92 ± 0.04	24.99 ± 0.06	1.93 ± 0.06
Deposition ($Tg\,yr^{-1}$)	45.1 ± 3.1 (11 %)	53.4 ± 2.0 (20 %)		3303.2 ± 41.5 (73 %)
Residence time (days)	8.4 ± 0.4	6.2 ± 0.1		0.2 ± 0.0
	Mineral dust		Mineral dust ($< 10\,\mu m$)	
Emissions ($Tg\,yr^{-1}$)	2484.1 ± 211.8	10142.0 ± 294.2	848.2 ± 94.9	3302.1 ± 41.5
Burden (Tg)	8.4 ± 1.4	28.34 ± 1.57	8.2 ± 1.3	27.13 ± 1.55
Deposition ($Tg\,yr^{-1}$)	2185.2 ± 190.0 (88 %)	10132.8 ± 296.0 (88 %)	846.2 ± 94.6 (69 %)	3243.3 ± 138.1 (65 %)
Residence time (days)	1.4 ± 0.1	1.0 ± 0.0	3.5 ± 0.2	3.0 ± 0.1

at 0.074 (64 %). This mode is mostly composed of sea-salt and sulphate. CLASSIC mineral dust AOD is 0.010 in the simulation that uses CLASSIC for the remaining aerosol species, 0.022 in the simulation that uses GLOMAP-mode.

Figure 2 shows distributions of total AOD at 0.55 µm averaged for 2003–2006, the last four years of the simulated period. Although mineral dust differs between the HadGEM2 and HadGEM3 simulations for the technical reasons stated in Sect. 3, those differences are not relevant to this study and would divert attention from actual differences between CLASSIC and GLOMAP-mode. Therefore, mineral dust AOD is hereafter taken from the HadGEM3 simulation only. The period 2003–2006 is selected to allow the comparison against total AOD in the MACC (Monitoring Atmosphere Composition and Climate) re-analysis, also shown in Fig. 2. The MACC re-analysis uses an aerosol model (Morcrette et al., 2009) embedded into the European Centre for Medium-Range Weather Forecasts (ECWMF) Integrated Forecast System (IFS) model. Benedetti et al. (2009) describe the IFS four-dimensional variational assimilation system that assimilates Moderate Resolution Imaging Spectroradiometer (MODIS) total AOD at 0.55 µm, thus correcting the modelled total AODs for departure from observations. Benedetti et al. (2009) also show by comparing to measurements at 41 ground-based sun-photometer sites that the reanalysis is more skilful than the free-running IFS aerosol model, being on average closer to the observations and displaying a lower bias and root-mean square error.

Although CLASSIC and GLOMAP-mode global-averaged AODs are similar, their distributions are different. CLASSIC produces larger AODs over oceans, over biomass-burning regions of Africa and South America, and over the Ganges Valley and China. GLOMAP-mode produces larger AODs over Northern Hemisphere continents, and at high latitudes of the Northern and Southern Hemispheres. Differences in the Southern Hemisphere are due to a southward shift in sea-salt AODs between CLASSIC, where sea-salt is not transported, and GLOMAP-mode. Compared to MACC, both CLASSIC and GLOMAP-mode underestimate the global-averaged AOD by about 30 %, mainly because of underestimated AODs over ocean and South Asia. CLASSIC overestimates AODs in the Eastern Pacific because of sea-salt and sulphate aerosols, the latter being produced from oxidation of ocean-based dimethyl sulphide emissions. Biomass-burning AODs in Africa and the Atlantic differ between the two schemes. CLASSIC tends to overestimate AODs compared to MACC in those regions, while GLOMAP-mode underestimates. Smaller biomass-burning AODs in GLOMAP-mode are due to the shorter residence time of carbonaceous aerosols and longer rate of condensation of volatile organic compounds. The latter is prescribed to be an e-folding time of only 6 h in CLASSIC, thus producing a fast increase in mass of biomass-burning particles. At high Northern Hemisphere latitudes, GLOMAP-mode AODs are overestimated compared to MACC because of the long residence time of sulphate aerosols in that scheme. However, it is worth noting

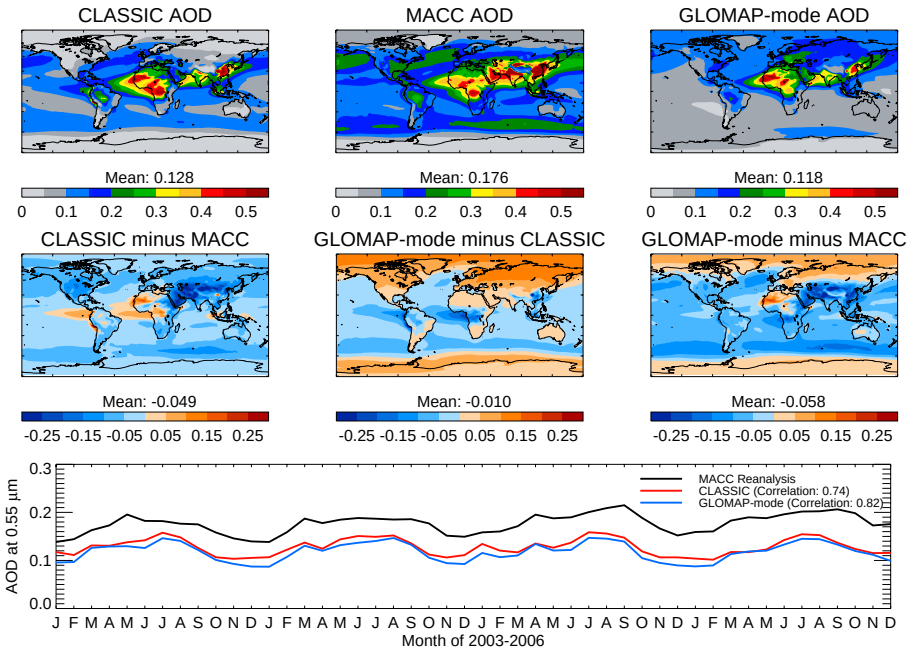

Fig. 2. Top row: total aerosol optical depth (AOD) at 0.55 µm for the period 2003–2006 in, from left to right, HadGEM using the CLASSIC aerosol scheme, the MACC aerosol re-analysis, and HadGEM using the GLOMAP-mode aerosol scheme. Middle row: differences between, from left to right, CLASSIC and MACC, GLOMAP-mode and CLASSIC, and GLOMAP-MODE and MACC. Bottom row: timeseries of global, monthly-averaged aerosol optical depth at 0.55 µm in the MACC aerosol re-analysis (black), CLASSIC (red), and UKCA-MODE (blue) for 2003–2006.

that satellite data available for assimilation in high-latitude regions are sparse and MACC may not reflect actual aerosol distributions there. Figure 2 also shows the interannual variability in monthly total AOD over the period 2003–2006. Both CLASSIC and GLOMAP-mode reproduce the seasonality in AOD, which peaks in Northern Hemisphere summer, but GLOMAP-mode achieves a better correlation with MACC.

Total AODs at 0.44 µm measured by ground-based sunphotometers in the Aerosol Robotic Network (AERONET) (Holben et al., 2001) are used for a more quantitative assessment, as shown in Fig. 3. The assessment procedure uses the 135 AERONET sites that provide at least 24 valid monthly averages of level 2 version 2 quality over the period 2000–2006. Corresponding timeseries of CLASSIC and GLOMAP-mode AODs are then extracted at each site. Again, the mineral dust AOD from HadGEM3 is shared by both simulations in order to isolate the changes in aerosol scheme. Lastly, model skill is computed against AERONET timeseries as the root-mean square error (RMSE), which quantifies the ability to reproduce the magnitude of AODs, and correlation, which quantifies the ability to reproduce the seasonal and interannual variability. A skilful simulation has low RMSE and high correlation against AERONET. Examples of AERONET and modelled timeseries are shown on the top and bottom rows of Fig. 3. Model skills depends on the site. For GLOMAP-mode, RMSEs are lower than 0.1 and correlations better than 0.6 across North American and European sites. Timeseries at GSFC (Maryland) and Lille (France) show that models reproduce well the magnitude and seasonality of the AOD, although the summer peak is often underestimated. Interannual variability at those sites is low. RMSEs are larger, and correlations often lower, at sites dominated by biomass-burning and/or mineral dust in South America and Africa, which suggest limitations in the dataset of primary emissions of carbonaceous aerosols and shortcomings in the mineral dust emissions interactively calculated by the CLASSIC scheme. In Alta Floresta (Brazil), seasonality and interannual variability are well reproduced. However, GLOMAP-mode underestimates peak AOD, while CLASSIC simulates the right magnitude for some years. Correlations suffer from the early increase in AOD in both models, which may indicate issues with the timing of the biomass-burning emissions. In Banizoumbou, models tend to underestimate the AOD and, although they simulate interannual variations, these do not always match the observations. Skill is relatively poor in Asia, and limitations in the primary carbonaceous emission dataset may again play a role. In Kanpur (India), both models simulate deep seasonal minima in the AOD that are both lower than and out of phase with the observations. In spite of those flaws, GLOMAP-mode improves on CLASSIC: RMSE decreases by 4 % and correlation increases by 2 % when averaged over all sites. Improvements happen mostly in the

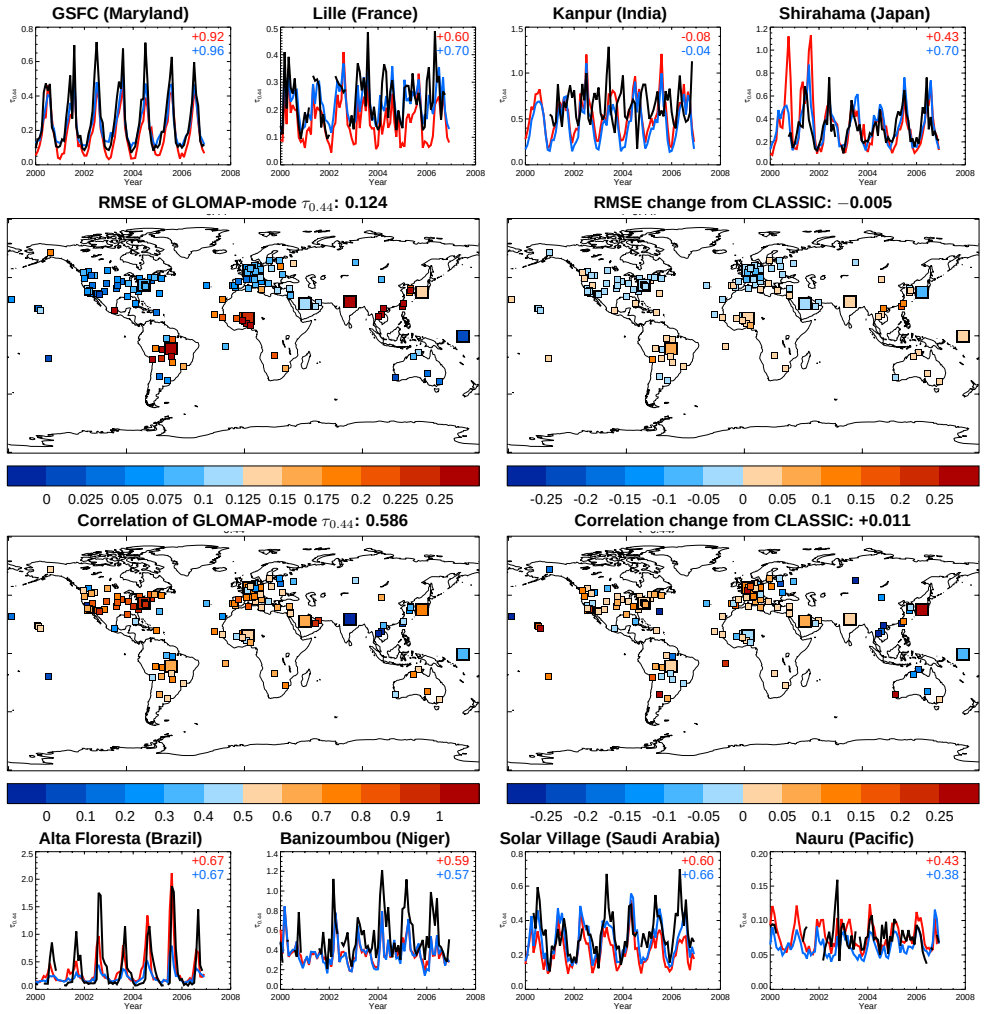

Fig. 3. Top and bottow rows: timeseries of monthly-averaged aerosol optical depths at 0.44 µm from AERONET (black), CLASSIC (red), and GLOMAP-mode (blue) for the period 2000–2006 at 8 AERONET sites worldwide. Numbers in the top right corner of each panel shows the correlation between AERONET measurements and CLASSIC (red) and GLOMAP-mode (blue) simulations. Second row, left: map of root mean square error (RMSE) of GLOMAP-mode 2000–2006 timeseries evaluated against observations at 135 AERONET sites. Number in panel title is the RMSE averaged over the 135 AERONET sites. Larger boxes identify the 8 sites shown in the top and bottom rows. Second row, right: map of changes in RMSE due to switching from CLASSIC to GLOMAP-mode aerosol schemes. Third row: as second row, but for the correlation.

Northern Hemisphere, while RMSE increases over most Southern Hemisphere sites. GLOMAP-mode also reduces the bias of modelled AOD against AERONET observations. Across the 135 AERONET sites, bias is −0.058 for CLASSIC and −0.039 for GLOMAP-mode, indicating a tendency to underestimate AOD in both schemes. GLOMAP-mode absolute bias is 0.065, smaller than the absolute bias of 0.074 achieved by CLASSIC.

5 Direct radiative effect

The HadGEM radiation schemes accounts for aerosol direct and semi-direct effects by computing aerosol optical properties averaged across 6 shortwave and 9 longwave bands. Optical properties are the specific scattering and absorption coefficients, in $m^2\,kg^{-1}$, which quantify the strength of scattering and absorption processes per unit aerosol mass, and the dimensionless asymmetry parameter, which describes in a simplified way the angular dependence of the scattering.

The CLASSIC aerosol scheme interactively simulates the dry aerosol mass. Each optically-active mode is associated with a prescribed lognormal size distribution of aerosol number, characterised by its modal radius and standard deviation, a set of wavelength-dependent complex refractive index, and a parameterisation of hygroscopic growth as a function of relative humidity, as detailed by Bellouin et al. (2011). Since those parameters are prescribed, monochromatic aerosol

optical properties are first computed offline by Mie calculations, then averaged across shortwave and longwave bands and stored for use when HadGEM is run.

Compared to CLASSIC, the GLOMAP-mode scheme introduces three important changes relevant to the radiation scheme. First, the mean radius of the modal size distributions varies interactively. Second, the modal refractive index depends on the internal composition of the mode. Third, the amount of aerosol water in each soluble mode varies interactively. Consequently, it is not possible to obtain the aerosol optical properties prior to a model run. However, to avoid running expensive monochromatic Mie calculations at runtime, optical properties are pre-computed for all realistic combinations of Mie parameter (modal radius normalised to the wavelength) and refractive index. To simplify those pre-computations, standard deviations of the lognormal size distributions are fixed at 1.59 for Aitken and accumulation modes, and 2 for coarse modes. The interaction of nucleation mode particles with radiation is neglected, since their optical properties are comparable to those of the more numerous gas-phase molecules. At runtime, when modal median radius and chemical composition are known, the modal refractive index is computed as the volume-weighted average of the refractive index of components residing in the mode, including water for soluble modes. Stier et al. (2007) have shown that different methods used to compute refractive index, including simple volume weighting, yield aerosol absorptions that agree within 15 %. The sets of component refractive index used in this calculation are the same as for CLASSIC aerosols, documented in Table A1 of Bellouin et al. (2011).

5.1 Aerosol absorption

Aerosol absorption depends on how aerosols are included in radiative transfer calculations. CLASSIC absorption is prescribed globally. Fossil-fuel black carbon aerosols have a single-scattering albedo (SSA) of 0.41 at 0.55 µm, while aged fossil-fuel organic carbon and biomass-burning aerosols have SSAs of 0.98 and 0.93 at 60 % relative humidity, respectively. GLOMAP-mode absorption depends on the relative contribution of black and organic carbon aerosols to the internal modal mixture. SSA distributions in the 2000–2006 hindcast simulations are shown in Fig. 4. They differ greatly between the two models. At high latitudes and in the Arctic especially, CLASSIC shows SSA as low as 0.84. This is because total AOD in those regions is both small (Fig. 2) and dominated by black-carbon aerosol. GLOMAP-mode aerosols are scattering at high latitudes, with a SSA close to 1. Although the lack of measurements in those regions make aerosol absorption difficult to validate, it is expected that the long residence time of CLASSIC black-carbon causes excessive transport to high latitudes and wrongly lowers the aerosol SSA. Elsewhere, continental aerosol absorption is relatively uniform in CLASSIC, with SSAs ranging from 0.94 to 0.96. In GLOMAP-mode, South Asia and biomass-burning regions of South America and Africa stand out as being more absorbing, with SSAs between 0.90 and 0.96. In those regions, validation can rely on ground-based measurements. Dubovik et al. (2002) obtain values ranging from 0.87 to 0.94 from an analysis of sun-photometer inversions of SSA values at AERONET sites dominated by biomass-burning aerosols, with African sites suggesting more absorption than South American sites. Aircraft measurement of aerosol absorption in the ageing biomass-burning plume off South Africa suggest a SSA of 0.90 (Abel et al., 2003). GLOMAP-mode represents the contrast between South American and African biomass-burning absorption better than CLASSIC.

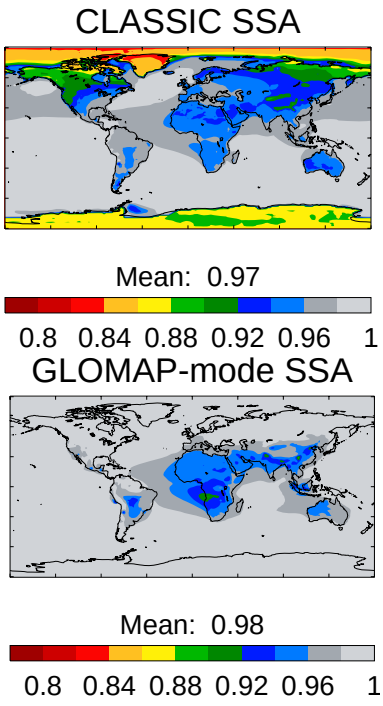

Fig. 4. Aerosol single-scattering albedo (SSA) at 0.55 µm, integrated over the atmospheric column and averaged over the period 2000–2006 for CLASSIC (top) and GLOMAP-mode (bottom).

6 Indirect radiative effect

In HadGEM, cloud condensation nuclei (CCN) enter the calculation of the cloud droplet number concentration (CDNC), made using the empirical relationship by Jones et al. (2001):

$$\mathrm{CDNC} = 3.75 \times 10^{8} \left(1 - \exp\left(-2.5 \times 10^{-9} \mathrm{CCN}\right)\right) \qquad (1)$$

where CDNC and CCN are given in m^{-3}. A minimum CDNC of $5 \times 10^{6}\,\mathrm{m}^{-3}$ is enforced by the model. CDNC is then used in the calculation of cloud albedo to represent the

first indirect effect and of autoconversion rates to represent the second indirect effect.

CLASSIC and GLOMAP-mode differ in their calculation of CCN. CLASSIC CCN is assumed equal to the number of aerosols in the accumulation and dissolved modes. Aerosol number is computed from the aerosol mass and prescribed size distributions. Mineral dust and fossil-fuel black carbon aerosols are assumed not to contribute to CCN. In contrast, GLOMAP-mode modal aerosol number is simulated independently of aerosol mass. GLOMAP-mode CCN is also a subset of aerosol number, but includes more particles than CLASSIC. The modal scheme calculates CCN as the number concentration of soluble mode particles that have dry radii larger than an activation dry radius, set to 37.5 nm in the HadGEM configuration (Mann et al., 2010). Doing so includes accumulation and coarse mode particles, but also part of the Aitken mode.

6.1 Response of CCN to changes in DMS

Dimethyl sulphide (DMS) is a biogenic gas produced by phytoplankton in the surface ocean. Once in the atmosphere, DMS is oxidized, and contributes to sulphate aerosol. Charlson et al. (1987) outlined a climate feedback linking DMS emission to the aerosol indirect effects and climate. Here, a uniform global increase in DMS flux of 25 % was applied to both aerosol schemes in order to test the CCN response. The model configuration used for this experiment differs slightly from the experiments noted so far in that both CLASSIC and GLOMAP-mode are run in parallel in the same simulation. The CCN response is measured in terms of CCN sensitivity, defined in Woodhouse et al. (2010) as $\Delta \mathrm{CCN}_{\mathrm{abs}} / \Delta \mathrm{Flux}_{\mathrm{DMS,abs}}$.

Figure 5 shows the calculated CCN sensitivity in CLASSIC and GLOMAP-mode. In all three spatial domains (global, Northern Hemisphere and Southern Hemisphere) the CCN response for a given DMS flux perturbation is approximately a factor of four greater in CLASSIC than in GLOMAP-mode. The CLASSIC aerosol scheme will therefore have a stronger Charlson et al. (1987) feedback compared to GLOMAP-mode.

The difference in CCN sensitivities between the two aerosol schemes can be explained in terms of the different microphysical representations. Figure 5 shows schematically how each aerosol scheme responds to an increase in DMS flux. Both observations and modelling have shown that the dominant source of sulphate is through aqueous-phase oxidation in the presence of stratocumulus clouds (Andreae et al., 1999; O'Dowd et al., 1999; Yang et al., 2011; Woodhouse et al., 2013). The CLASSIC scheme, which does not simulate aerosol number and assumes a fixed modal distribution for sulphate aerosol, is only able to respond to an increase in sulphur by directly increasing the CCN number (label "a" in Fig. 5). By contrast, GLOMAP-mode is able to increase the geometric mean diameter of its modes (label "b" in Fig. 5) in

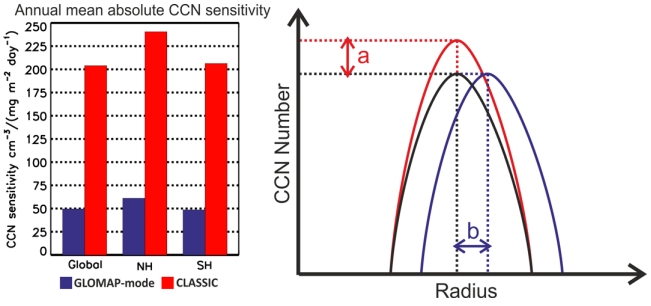

Fig. 5. Left panel: annual mean CCN sensitivity (global, Northern Hemisphere and Southern Hemisphere) for GLOMAP-mode and CLASSIC. Right panel: idealized responses to the same sulphur perturbation in the two different schemes. See text for details.

response to additional sulphate (e.g. through aqueous-phase oxidation). The GLOMAP-mode response is more realistic, as aqueous-phase oxidation only grows existing CCN, and does not create new CCN (Woodhouse et al., 2013). Note however that GLOMAP-mode does create a limited number of new CCN via nucleation and condensational growth resulting from the extra sulphur. This comparison suggests that the climate feedback from DMS is too high in HadGEM2-ES simulations using CLASSIC. CLASSIC and GLOMAP-mode also produce quite different spatial responses, which are not discussed further here.

The different CCN sensitivities highlighted here are in response to a DMS flux perturbation. However, the findings are equally valid for other changes in the source of sulphur dioxide, from anthropogenic sources for example. Such changes are investigated in the next section.

7 Aerosol radiative forcing

Aerosol radiative forcing is diagnosed by calling the radiation scheme twice in order to suppress the model response to aerosol radiative effects, a configuration called double-call simulation. The first call includes aerosol radiative effects. The second call does not and is used to advance the model into its next time step. The difference in radiative fluxes between the two calls provides the aerosol radiative perturbation with respect to an atmosphere containing no aerosols. The difference between two parallel double-call simulations with aerosol and precursor emissions set to 1850 and 2000 levels provides the aerosol forcing exerted by changes in aerosol concentrations between the two years. All other forcing agents, such as greenhouse gases or land-use change, remain fixed at their 2000 levels. Because the AeroCom Hindcast dataset of aerosol and precursor emissions used so far in this study only covers the period 1980 to 2006, double-call simulations use years 1850 and 2000 of the CMIP5 historical emission datasets (Lamarque et al., 2010). Meteorology is independent of the aerosols included in double-call

simulations, and is nudged to year 2006. Aerosol emissions that are driven by simulated meteorology, such as for mineral dust and sea-salt aerosols, are the same in the two parallel double-call simulations and exert no radiative forcing, by construction. In addition, only direct and first indirect radiative forcing can be diagnosed by suppressing the model response to aerosol radiative effects. Semi-direct and second indirect radiative forcings imply modifications to clouds which prevent the tropospheric state from being held fixed. In the following, aerosol radiative forcing refers to the sum of direct and first indirect forcing only.

In spite of sharing the same emission datasets, CLASSIC and GLOMAP-mode simulate different distributions of total AOD at 0.55 µm for the years 1850 and 2000. Differences for the year 2000 are similar to those shown in Fig. 2 and discussed in Sect. 4. Differences for the year 1850 are shown in Fig. 6. They are qualitatively similar to those for the year 2000 over most of the globe: larger AODs over oceans and biomass-burning region in CLASSIC, and a southward shift of sea-salt AODs in the Southern Hemisphere. For present-day aerosols, GLOMAP-mode features large AODs over the mid- and high-latitudes of the Northern Hemisphere that were attributed to the long residence time of sulphate aerosols. Those large AODs have completely disappeared in 1850, and both schemes simulate similar magnitudes of AOD in those regions, since anthropogenic emissions of sulphur dioxide in the CMIP5 dataset are only $1\,\mathrm{Tg[S]\,yr^{-1}}$ in 1850, compared to $52\,\mathrm{Tg[S]\,yr^{-1}}$ in 2000. Consequently, the differences in sulphur dioxide oxidation and residence time of sulphate aerosol between the two schemes have much less of an impact in 1850.

Figure 6 also shows distributions of column-integrated CDNC over the lowermost 10 km of the atmosphere for the year 1850, as simulated from CLASSIC and GLOMAP-mode aerosols, and their difference. With 1850 aerosol and precursor emissions, GLOMAP-mode aerosols produce 4.7 times more CDNCs than CLASSIC aerosols. Regions of relative maxima in CDNC are the same in both schemes, and correspond to areas where biomass-burning emissions are large: Southeastern United States, South America, Central Africa, and India. The Andes, Mediterranean, and Indonesia also stand out because of large sulphur dioxide emissions from degassing volcanoes. The distribution of the difference in CDNC between CLASSIC and GLOMAP-mode is relatively uniform, and background CDNC is therefore the main difference. GLOMAP-mode simulates a background CDNC that is at least $30 \times 10^6\,\mathrm{cm^{-2}}$ larger than CLASSIC. The representation of the source of CCN from nucleated particles entrained into the boundary layer in GLOMAP-mode explains the larger background. In mass-based schemes such as CLASSIC, this source of CCN is essentially absent since nucleation is neglected. These nucleated "secondary CCNs" are mostly in the size range between 0.05 and 0.08 µm. They are therefore efficient CCNs but contribute very little to AOD as those sizes are much shorter than the wavelengths where solar radiation peaks. Those results are consistent with Merikanto et al. (2009), who showed that in marine regions, where aerosol indirect forcing is mostly exerted, more than half of CCN are actually nucleated particles.

Figure 7 shows distributions of the difference in total AOD at 0.55 µm between years 2000 and 1850, also termed anthropogenic AOD, and the direct forcing exerted by that change. Looking at anthropogenic AOD is relevant since direct forcing increases approximately linearly with that quantity (Boucher et al., 1998). In spite of sharing the same emission datasets with CLASSIC, GLOMAP-mode produces an anthropogenic AOD that is 62 % larger, at 0.034 on a global and annual average, with larger values over most of the Northern Hemisphere. As discussed above, the enhanced impact of anthropogenic emissions in GLOMAP-mode is due to both the smaller AODs in 1850, and the longer residence time of sulphate aerosols in 2000. It follows that aerosol direct forcing is more strongly negative, by 70 % at $-0.49\,\mathrm{W\,m^{-2}}$, in GLOMAP-mode than in CLASSIC. The dependence of direct forcing on the availability of solar radiation and solar zenith angle explains why the additional anthropogenic optical depth strengthens the forcing mainly at mid-latitudes rather than uniformly across the Northern Hemisphere.

To better understand differences in total direct forcing between the two aerosol schemes, Fig. 8 shows distributions of direct forcing for individual anthropogenic aerosol species: sulphate, fossil-fuel black carbon, fossil-fuel organic carbon, and the combination of black and organic carbon from biomass-burning emissions. Those component direct forcings are obtained from sets of two parallel double-call simulations with sulphur dioxide emissions, or primary carbonaceous emissions, depending on the species of interest, set to 1850 and 2000 levels. Global, annual-averaged sulphate direct forcing is $-0.67\,\mathrm{W\,m^{-2}}$ in GLOMAP-mode, stronger than the $-0.28\,\mathrm{W\,m^{-2}}$ obtained in CLASSIC. A stronger forcing is the expected consequence of the larger burden and longer residence time of sulphate in GLOMAP-mode (see Table 2). In contrast, fossil-fuel black carbon direct forcing is weaker in GLOMAP-mode than in CLASSIC, at $+0.12$ and $+0.19\,\mathrm{W\,m^{-2}}$, respectively. Again, differences are explained by the different residence times. In CLASSIC, black carbon resides in the atmosphere for 15 days, allowing transport to the Arctic and across the Pacific and increasing the globally-averaged direct forcing. In GLOMAP-mode, black carbon residence time is only 5 days. Black carbon aerosols remain located over India and China and exert no direct forcing at high latitudes. Direct forcing of fossil-fuel organic carbon aerosols is weak and similar in CLASSIC, at $-0.04\,\mathrm{W\,m^{-2}}$, and GLOMAP-mode, at $-0.03\,\mathrm{W\,m^{-2}}$, because both schemes simulate similar burdens. Finally, direct forcing from primary carbonaceous emissions due to biomass burning is $-0.07\,\mathrm{W\,m^{-2}}$ in CLASSIC, stronger than the $0.00\,\mathrm{W\,m^{-2}}$ obtained in GLOMAP-mode. In addition to the larger AODs obtained in CLASSIC over biomass-burning regions (Fig. 2), differences in aerosol absorption

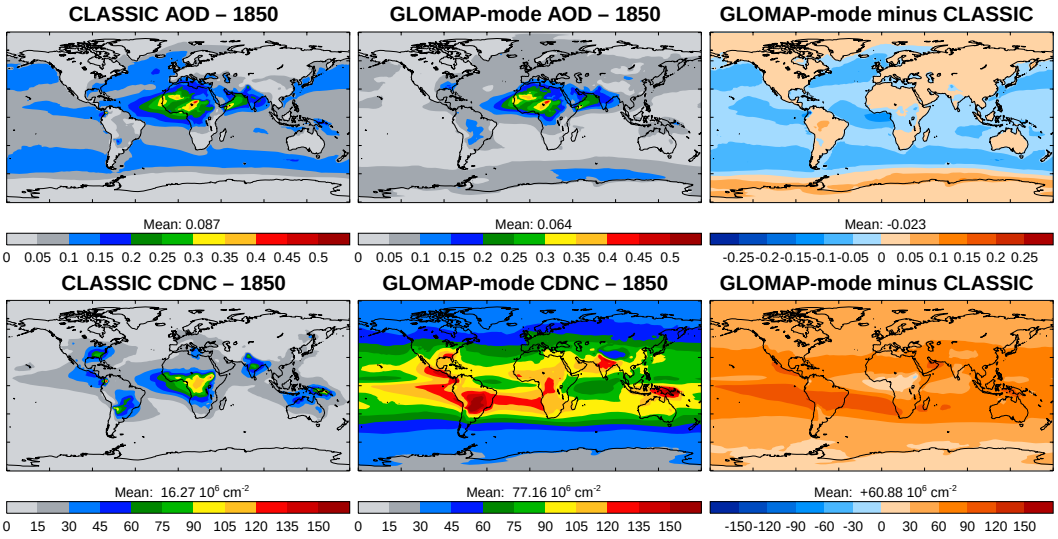

Fig. 6. Top row: aerosol optical depth (AOD) at 0.55 µm in CLASSIC (left), GLOMAP-mode (middle) and their difference (right). Bottom row: same as top row, but for the column-integrated cloud droplet number concentration (CDNC), in 10^6 cm^{-2}. CDNC is integrated over the lowermost 10 km of the atmosphere. All simulations use aerosol and precursor emissions for the year 1850.

(Fig. 4) also play a role. Specifically, the moderately absorbing CLASSIC biomass-burning aerosols exert a neutral direct forcing over the stratocumulus deck off the Atlantic shores of Southern Africa. The increased absorption in GLOMAP-mode makes direct forcing strongly positive in the same region. Note that the positive biomass-burning direct forcing obtained by CLASSIC and GLOMAP-mode over the Southeastern United States is a consequence of the CMIP5 biomass-burning emissions, which are larger in 1850 than in 2000: the associated decrease in biomass-burning aerosol concentrations translates into a positive forcing. In summary, the more strongly negative total direct forcing in GLOMAP-mode is a consequence of the stronger direct forcing by sulphate aerosols. Differences in globally-averaged direct forcing between CLASSIC and GLOMAP-mode are however partly reduced by the positive forcing due to black carbon at high latitudes in CLASSIC, and the more positive forcing exerted in cloudy-sky by the more absorbing biomass-burning aerosol in GLOMAP-mode.

For aerosol-cloud interactions, Fig. 7 shows distributions of changes in column-integrated CDNC between the years 2000 and 1850, and the first indirect forcing thus exerted. Here, changes are expressed in terms of ratio of CDNC between the two years, since cloud susceptibility, defined as the change in cloud albedo due to a change in CDNC, is an exponentially decreasing function of CDNC (Taylor and McHaffie, 1994). Column integration covers the lowermost 10 km of the atmosphere where most liquid clouds are located. Both CLASSIC and GLOMAP-mode simulate large increases in CDNC due to anthropogenic emissions over the Northern Hemisphere, but differ in the magnitude of those increases, relative to background CDNC. CLASSIC shows large CDNC ratios, close to 2 on a global average and up to 13.1 locally. GLOMAP-mode shows smaller ratios, with a global average of 1.2 and a maximum of 2.5, in spite of having a longer residence time for sulphate aerosols. Here again, differences between CDNCs simulated with aerosol and precursor emissions for the year 1850 are important. As discussed above, GLOMAP-mode has a much higher background that CLASSIC, and the influence of the pre-existing CCNs translate into a reduced sensitivity of CDNC to anthropogenic aerosol emissions.

The analysis of the response of CDNC to DMS emissions changes, discussed in Sect. 6.1, can be generalised to changes in anthropogenic emissions. Firstly, in CLASSIC, the addition of aerosol mass automatically increases aerosol number, and eventually CCN and CDNC. In GLOMAP-mode, mass can be added to a pre-existing particle, thus not increasing total number and leading to a more modest increase in CDNC between 1850 and 2000. This is consistent with the result of Pringle et al. (2009), who have shown in their Fig. 5 that CDNC is more effectively increased by the addition of new particles (i.e. increasing aerosol number) than by condensation on to existing particles. Also, accounting for nucleation processes in GLOMAP-mode yields areas where CDNC is larger in 1850 than in 2000: nucleation is enhanced by conditions of low condensation sink of gas-phase species to existing aerosols. Low anthropogenic emissions in the year 1850 create such conditions, as discussed by Schmidt et al. (2012). They showed that continously degassing volcanoes increase pre-industrial CDNC by 40 % but present-day CDNC by only 10 %. According to the GLOMAP-mode simulation discussed in this paper, this global process is most apparent over South Hemisphere oceans where it exerts

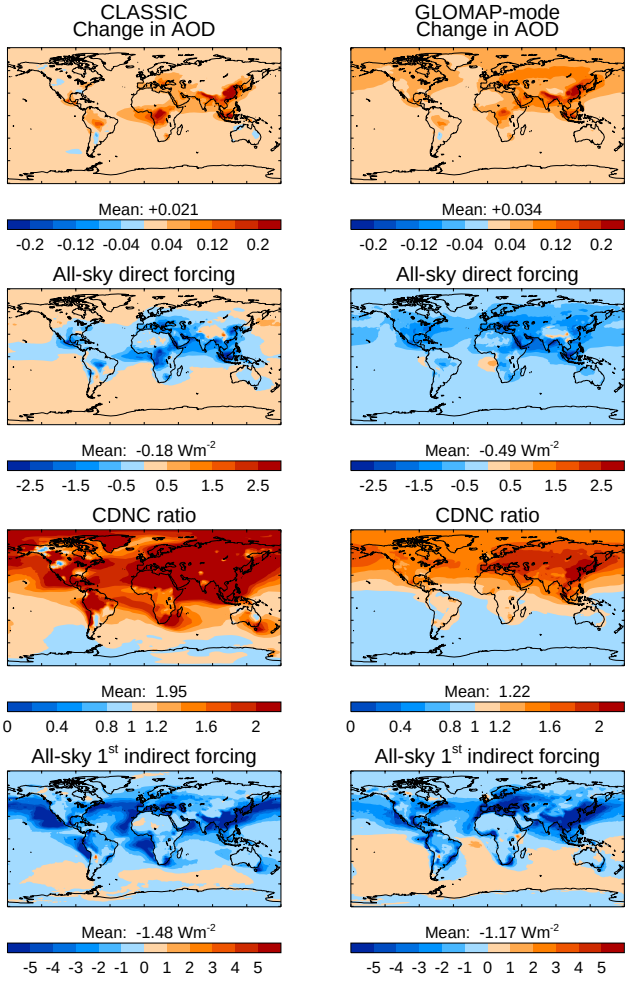

Fig. 7. Top row: change in total aerosol optical depth (AOD) between simulations with emissions for the years 2000 and 1850 using the CLASSIC (left) and GLOMAP-mode (right) aerosol scheme. Second row: all-sky direct radiative forcing at the top of the atmosphere (TOA), in $\mathrm{W\,m^{-2}}$. Third row: ratio between cloud droplet number concentration (CDNC) simulated with 2000 and 1850 emissions. CDNC is integrated over the lowermost 10 km of the atmosphere. Bottom row: all-sky first indirect radiative forcing at the TOA, in $\mathrm{W\,m^{-2}}$.

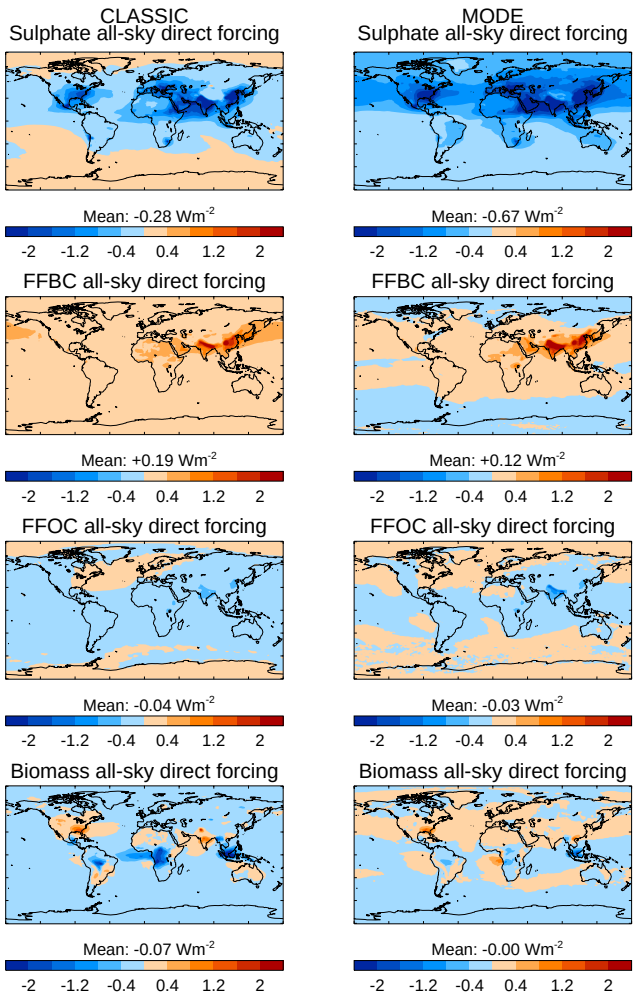

Fig. 8. All-sky shortwave direct radiative forcing at the top of the atmosphere, in $\mathrm{W\,m^{-2}}$, for 1850–2000 changes in (top to bottom) sulphate, fossil-fuel black carbon (FFBC), fossil-fuel organic carbon (FFOC), and biomass-burning aerosols, as simulated by the CLASSIC (left) and GLOMAP-mode (right) aerosol schemes.

a weak, positive first indirect forcing. Overall, clouds, and especially low maritime clouds, are less susceptible to aerosol changes in GLOMAP-mode than in CLASSIC. The lesser ability to change CDNC translates into a weaker first indirect forcing from GLOMAP-mode, at $-1.17\,\mathrm{W\,m^{-2}}$ compared to $-1.48\,\mathrm{W\,m^{-2}}$ in CLASSIC.

Coincidentally, both CLASSIC and GLOMAP-mode direct and first indirect forcings sum up to $-1.66\,\mathrm{W\,m^{-2}}$. However, first indirect forcing represents 89 % of that sum in CLASSIC and only 70 % in GLOMAP-mode. Because of this shift towards the direct forcing, regions of strong forcing have moved from the ocean in CLASSIC to land surfaces in GLOMAP-mode.

8 Conclusions

The analysis of differences between HadGEM simulations using the mass-based CLASSIC or the modal GLOMAP-mode aerosol schemes leads to the following key findings.

Over the period 2000–2006 the GLOMAP-mode modal aerosol scheme simulates AODs that compare better against aerosol ground-based observations and a data-assimilated aerosol re-analysis. In GLOMAP-mode, a longer sulphate residence time leads to increased total AOD in the Northern Hemisphere, while a shorter black carbon residence time increases the single-scattering albedo over high latitudes regions. CLASSIC produces larger AODs over oceanic and biomass-burning regions. The comparisons also highlight how simpler mass-based schemes have problems representing growth processes which should increase aerosol mass

without increasing aerosol number, such as aqueous sulphate production. This inherent limitation of mass-based aerosol scheme causes a substantially high bias in CCN sensitivity to changes in DMS. The finding suggests that the associated Earth System feedbacks simulated by climate models with such first-generation aerosol schemes are overestimated.

Distributions of AOD and CDNC for the year 1850 differ strongly. Low anthropogenic emission rates of sulphur dioxide in that year effectively suppress the impact of different sulphate aerosol residence times, while oceanic and biomass-burning differences remain. AOD for 1850 is therefore smaller with GLOMAP-mode than CLASSIC. In contrast, CDNC is almost 5 times larger in GLOMAP-mode. The microphysical scheme has higher 1850 CDNC since it includes nucleation, which provides an important source of new particles, and the coagulation and condensation processes which grow these secondary particles up to CCN sizes. The importance of adequately simulated aerosol properties in the year 1850 illustrates how present-day validation of simulated aerosols is only a weak test of model fidelity in estimating forcing. It also underlines the need for microphysical processes to be included in aerosol schemes within climate models to avoid biases in simulated indirect effects on climate. The finding leads to a recommendation that more effort should be made to evaluate models against observations in remote regions, since these are closest to the pre-industrial atmosphere. However, most regions are now influenced by anthropogenic aerosols to some extent, and the remaining pristine regions do not cover all cloud regimes.

The two-moment modal scheme simulates a stronger direct aerosol forcing of $-0.49\,\mathrm{W\,m^{-2}}$ on a global-, annual-average, compared to $-0.18\,\mathrm{W\,m^{-2}}$ for the mass-based scheme. The smaller 1850 baseline combined with the longer sulphate aerosol residence time increase the change in AOD between 1850 and 2000, and the direct forcing thus exerted. By contrast, the aerosol microphysics scheme simulates a weaker first indirect forcing at $-1.17\,\mathrm{W\,m^{-2}}$ compared to $-1.48\,\mathrm{W\,m^{-2}}$ for the mass-based scheme. The higher CDNC background in 1850 and the lesser ability to change CDNC simulated when nucleation is included via the microphysical scheme are the main causes here.

The findings lead to two further questions. First, does the use of GLOMAP-mode provide more confidence in the aerosol forcing estimates? Second, are past results obtained using CLASSIC challenged by the more sophisticated aerosol scheme?

Direct forcing is affected by limitations in both aerosol schemes. Underestimated wintertime AODs and long black carbon residence time cause an underestimate of the strength of direct forcing in CLASSIC. In contrast, the long sulphate residence time of GLOMAP-mode is likely to cause an overestimate if it proves to be incorrect. However, the addition of nitrate aerosols to the GLOMAP-mode scheme will also increase anthropogenic AOD. A future direct forcing estimate is therefore unlikely to be much weaker than the current $-0.5\,\mathrm{W\,m^{-2}}$. It is worth noting that this value is close to the best estimate of $-0.4\,\mathrm{W\,m^{-2}}$ proposed by Forster et al. (2007), although stronger than the observationally-adjusted estimate of $-0.3\,\mathrm{W\,m^{-2}}$ derived by Myhre (2009). The CLASSIC estimate of $-0.18\,\mathrm{W\,m^{-2}}$ is weaker than those numbers.

Aerosol microphysics schemes like GLOMAP-mode have been designed to dynamically simulate the evolution of the particle size distribution and hence simulate CCN independently of aerosol mass. By contrast, in a mass-based scheme like CLASSIC mass and number vary proportionally. This assumption, made at a time when model runtime costs had to be severely limited, is unsupported by observations and may lead to biases in simulated aerosol indirect forcings. It is therefore expected that GLOMAP-mode provides more robust foundations for studying aerosol indirect forcing. Indeed, CCN concentrations simulated by GLOMAP-mode have been successfully compared to observations (Mann et al., 2010). However, CCN has to be converted to CDNC to quantify indirect forcing. This study uses the empirical parameterisation by Jones et al. (2001) to make that conversion. More sophisticated and mechanistic approaches of aerosol activation have been proposed (Abdul-Razzak and Ghan, 2000) and are being implemented within the GLOMAP-mode framework. Those improvements may change the indirect forcing estimate in the future. The current GLOMAP-mode estimate of $-1.2\,\mathrm{W\,m^{-2}}$ lies in the middle of the range -0.3 to $-1.8\,\mathrm{W\,m^{-2}}$ assessed by Forster et al. (2007).

The GLOMAP-mode forcing estimates are better founded on physical principles of aerosol dynamics than the CLASSIC estimates. However, it is striking that the selection of one aerosol scheme over another can cause a near-doubling of direct forcing and a 20 % decrease in indirect forcing. Other mass-based aerosol schemes, such as those used in the recent CMIP5 climate simulations, are also likely to overestimate the indirect radiative forcings. Adding uncertainties on pre-industrial and present-day aerosol emissions, aerosol absorption, and indirect effect mechanisms, and accounting for limitations due to the host model would increase uncertainties beyond those assessed in the latest IPCC assessment report (Forster et al., 2007), especially for the direct forcing.

CLASSIC has been used within the Hadley Centre climate model for a long time and provided interesting results which are expected to be replicated with GLOMAP-mode. Roberts and Jones (2004) showed that fossil-fuel black carbon aerosols generate feedbacks on ice albedo, water vapour, and temperature and cloud profiles that are weaker than those generated by carbon dioxide. Although the value of black carbon climate sensitivity may depend on the aerosol scheme used, its weakness compared to carbon dioxide is based on the response by other components of the climate model. Specifically, the vertical profile of aerosol absorption, which is mainly driven by the tracer transport scheme, and the sign of cloud feedbacks will have more impact than the aerosol scheme. Jones et al. (2007) found by using a prototype

version of HadGEM2 that the temperature response to sulphate and black carbon aerosol forcings is mainly located in the Northern Hemisphere, a different pattern from the response by biomass-burning aerosols and carbon dioxide, which are globally symmetric. These patterns are driven by anthropogenic emissions and are qualitatively replicated in GLOMAP-mode. Andrews et al. (2010) showed that the precipitation response to various forcing agents, including CLASSIC aerosols, can be split into a fast atmospheric response that is correlated with the atmospheric radiative forcing, and a slower response to global surface temperature change that is independent of forcing mechanism. Although GLOMAP-mode would provide a different atmospheric radiative forcing, especially for absorbing aerosols, precipitation responses would be qualitatively similar. Jones et al. (2011) detected the contribution of fossil-fuel black carbon aerosols to global warming for periods in the twentieth century by using HadGEM1. The long residence time of black carbon in CLASSIC is not an issue for pattern-based detection and attribution techniques, which are able to identify biases in the strength of the various forcings they include. However, the positive forcing by CLASSIC black carbon aerosols over the Arctic is likely to have compensated for the lack of representation of the forcing due to black carbon deposition on ice and snow in that model. Reproducing the result using GLOMAP-mode will require the addition of the forcing due to black-carbon deposition on snow in order to maintain the overall forcing pattern.

In contrast, other past results will be more directly affected by the change in aerosol scheme. Bellouin et al. (2011) documented historical and future aerosol forcing in the CMIP5 simulations by HadGEM2-ES. As shown in this study, aerosol forcing depends on the aerosol scheme used, and GLOMAP-mode distributes the forcing differently among direct and indirect effects. Two additional results of Bellouin et al. (2011) include the increase in the contribution of nitrate aerosols to aerosol forcing in the future, and the increase in aerosol residence time as low-cloud cover decreases with global warming, slowing down wet deposition. The first result would be replicated in GLOMAP-mode since it depends on the relative changes in sulphur dioxide and ammonia emissions in future scenarios. The second result should also be replicated, provided that the wet deposition scheme uses simulated, rather than prescribed, precipitation rates. Finally, the HadGEM2-ES CMIP5 historical simulation was shown by Booth et al. (2012) to replicate better the multi-decadal oscillation of sea-surface temperatures in the Atlantic than older models. The improved skill was traced back to the strong indirect forcing exerted by anthropogenic aerosols over the North Atlantic. Figure 7 suggests that the weaker indirect forcing obtained from GLOMAP-mode in that region will make that result difficult to replicate, unless an improved activation scheme increases the change in CDNC for maritime clouds.

In addition to providing improved comparison against observed AOD distributions, GLOMAP-mode represents microphysical processes that open opportunities for new science. The scheme has been used in a chemistry-transport model to show that, on the one hand, secondary aerosols derived from nucleation, a process not represented in CLASSIC, account for 45 % of low-cloud CCN (Merikanto et al., 2009). On the other hand, GLOMAP-mode also showed that changes in CCN are not very sensitive to changes in nucleation rates (Spracklen et al., 2008). Finally, the ability of GLOMAP-mode to represent atmospheric nucleation of aerosols allow the study of the potentially large impact of ammonia and organic species on the nucleation rate of sulphur acid particles (Kirkby et al., 2011). Improvements to GLOMAP-mode planned for the near future include the inclusion of nitrate aerosols and stratospheric chemistry and aerosols.

Acknowledgements. The contribution of Met Office Hadley Centre authors to this work was supported by the Joint DECC/Defra Met Office Hadley Centre Climate Programme (GA01101). GM is supported by the Natural Environment Research Council (NERC) through the National Centre for Atmospheric Science (NCAS). MTW was funded by a National Environment Research Council UK-SOLAS CASE studentship with the Met Office. The development of GLOMAP-mode within HadGEM is part of the UKCA project, which is supported by both NERC and the Joint DECC/Defra Met Office Hadley Centre Climate Programme. Funding by the European Union Framework Program 6 project European Aerosol Cloud Climate and Air Quality Interactions (EUCAARI), and Framework Program 7 projects Monitoring of Atmospheric Composition and Climate (MACC) and The Pan-European Gas Aerosol Climate Interaction Study (PEGASOS) is also acknowledged. The authors thank the AERONET principal investigators and their staff for establishing and maintaining the 135 sites used in this study.

Edited by: V.-M. Kerminen

References

Abdul-Razzak, H. and Ghan, S. J.: A parameterization of aerosol activation: 2. Multiple aerosol types, J. Geophys. Res., 105, 6837–6844, doi:10.1029/1999JD901161, 2000.

Abel, S. J., Haywood, J. M., Highwood, E. J., Li, J., and Buseck, P. R.: Evolution of biomass-burning aerosol properties from an agricultural fire in Southern Africa, Geophys. Res. Lett., 30, 1783, doi:10.1029/2003GL017342, 2003.

Adams, P. J. and Seinfeld, J. H.: Predicting global aerosol size distributions in general circulation models, J. Geophys. Res., 107, 4370, doi:10.1029/2001JD001010, 2002.

Andreae, M. O., Elbert, W., Cai, Y., Andreae, T. W., and Gras, J.: Non-sea-salt sulfate, methanesulfonate, and nitrate aerosol concentrations and size distributions at Cape Grim, Tasmania, J. Geophys. Res., 104, 21695–21706, 1999.

Andrews, T., Forster, P. M., Boucher, O., Bellouin, N., and Jones, A.: Precipitation, radiative forcing and global

temperature change, Geophys. Res. Lett., 37, L14701, doi:10.1029/2010GL043991, 2010.

Bauer, S. E., Wright, D. L., Koch, D., Lewis, E. R., McGraw, R., Chang, L.-S., Schwartz, S. E., and Ruedy, R.: MATRIX (Multiconfiguration Aerosol TRacker of mIXing state): an aerosol microphysical module for global atmospheric models, Atmos. Chem. Phys., 8, 6003–6035, doi:10.5194/acp-8-6003-2008, 2008.

Bellouin, N., Jones, A., Haywood, J., and Christopher, S.: Updated estimate of aerosol direct radiative forcing from satellite observations and comparison against the Hadley Centre climate model, J. Geophys. Res., 113, D10205, doi:10.1029/2007JD009385, 2008.

Bellouin, N., Rae, J., Jones, A., Johnson, C., Haywood, J., and Boucher, O.: Aerosol forcing in the Climate Model Intercomparison Project (CMIP5) simulations by HadGEM2-ES and the role of ammonium nitrate, J. Geophys. Res., 116, D20206, doi:10.1029/2011JD016074, 2011.

Benedetti, A., Morcrette, J.-J., Boucher, O., Dethof, A., Engelen, R. J., Fisher, M., Flentje, H., Huneeus, N., Jones, L., Kaiser, J. W., Kinne, S., Mangold, A., Razinger, M., Simmons, A. J., and Suttie, M.: Aerosol analysis and forecast in the ECMWF Integrated Forecast System: 2. Data assimilation, J. Geophys. Res., 114, D13205, doi:10.1029/2008JD011115, 2009.

Bond, T. C., Streets, D. G., Fernandes, S. D., Nelson, S. M., Yarber, K. F., Woo, J.-H., and Klimont, Z.: A technology-based global inventory of black and organic carbon emissions from combustion, J. Geophys. Res., 109, D14203, doi:10.1029/2003JD003697, 2004.

Booth, B. B. B., Dunstone, N. J., Halloran, P. R., Andrews, T., and Bellouin, N.: Aerosols implicated as a prime driver of twentieth-century North Atlantic climate variability, Nature, 484, 228–233, doi:10.1038/nature10946, 2012.

Boucher, O., Schwartz, S. E., Ackerman, T. P., Anderson, T. L., Bergstrom, B., Bonnel, B., Chylek, P., Dahlback, A., Fouquart, Y., Fu, Q., Halthore, R. N., Haywood, J. M., Iversen, T., Kato, S., Kinne, S., Kirkevag, A., Knapp, K. R., Lacis, A., Laszlo, I., Mishchenko, M. I., Nemesure, S., Ramaswamy, V., Roberts, D. L., Russell, P., Schlesinger, M. E., Stephens, G. L., Wagener, R., Wang, M., Wong, J., and Yang, F.: Intercomparison of models representing direct shortwave radiative forcing by sulfate aerosols, J. Geophys. Res., 103, 16979–16998, 1998.

Carslaw, K. S., Boucher, O., Spracklen, D. V., Mann, G. W., Rae, J. G. L., Woodward, S., and Kulmala, M.: A review of natural aerosol interactions and feedbacks within the Earth system, Atmos. Chem. Phys., 10, 1701–1737, doi:10.5194/acp-10-1701-2010, 2010.

Charlson, R. J., Lovelock, J. E., Andreae, M. O., and Warren, S. G.: Oceanic phytoplankton, atmospheric sulfur, cloud albedo and climate, Nature, 326, 655–661, 1987.

Chipperfield, M. P.: New version of the TOMCAT/SLIMCAT Off-Line Chemical Transport Model: intercomparison of stratospheric tracer experiments, Q. J. R. Meteorol. Soc., 132, 1179–1203, doi:10.1256/qj.05.51, 2006.

Collins, W. J., Bellouin, N., Doutriaux-Boucher, M., Gedney, N., Halloran, P., Hinton, T., Hughes, J., Jones, C. D., Joshi, M., Liddicoat, S., Martin, G., O'Connor, F., Rae, J., Senior, C., Sitch, S., Totterdell, I., Wiltshire, A., and Woodward, S.: Development and evaluation of an Earth-System model – HadGEM2, Geosci. Model Dev., 4, 1051–1075, doi:10.5194/gmd-4-1051-2011, 2011.

Diehl, T., Heil, A., Chin, M., Pan, X., Streets, D., Schultz, M., and Kinne, S.: Anthropogenic, biomass burning, and volcanic emissions of black carbon, organic carbon, and SO2 from 1980 to 2010 for hindcast model experiments, Atmos. Chem. Phys. Discuss., 12, 24895–24954, doi:10.5194/acpd-12-24895-2012, 2012.

Dubovik, O., Holben, B., Eck, T. F., Smirnov, A., Kaufman, Y. J., King, M. D., Tanré, D., and Slutsker, I.: Variability of absorption and optical properties of key aerosol types observed in worldwide locations. J. Atmos. Sci., 59, 590–608, 2002.

Easter, R. C., Ghan, S. J., Zhang, Y., Saylor, R. D., Chapman, E. G., Laulainen, N. S., Abdul-Razzak, H., Leung, R., Bian, X., and Zaveri, R. A.: MIRAGE: model description and evaluation of aerosols and trace gases, J. Geophys. Res., 109, D20210, doi:10.1029/2004JD004571, 2004.

Eyring, V., Kohler, H. W., van Aardenne, J., and Lauer, A.: Emissions from international shipping: 1. The last 50 years, J. Geophys. Res., 110, D17305, doi:10.1029/2004JD005619, 2005a.

Eyring, V., Kohler, H. W., Lauer, A., and Lemper, B.: Emissions from international shipping: 2. Impact of future technologies on scenarios until 2050, J. Geophys. Res., 110, D17306, doi:10.1029/2004JD005620, 2005b.

Forster, P., Ramaswamy, V., Artaxo, P., Berntsen, T., Betts, R., Fahey, D. W., Haywood, J., Lean, J., Lowe, D. C., Myhre, G., Nganga, J., Prinn, R., Raga, G., Schulz M., and Van Dorland, R.: Changes in atmospheric constituents and in radiative forcing. In: Climate Change 2007: The Physical Science Basis. Contribution of Working Group I to the Fourth Assessment Report of the Intergovernmental Panel on Climate Change, edited by: Solomon, S., Qin, D., Manning, M., Chen, Z., Marquis, M., Averyt, K. B., Tignor, M., and Miller, H. L., Cambridge University Press, Cambridge, UK and New York, NY, USA, 2007.

Ghan, S., Laulainen, N., Easter, R., Wagener, R., Nemesure, S., Chapman, E., Zhang, Y., and Leung, R.: Evaluation of aerosol direct radiative forcing in MIRAGE, J. Geophys. Res., 106, 5295–5316, 2001.

Holben, B. N., Tanré, D., Smirnov, A., Eck, T. F., Slutsker, I., Abuhassan, N., Newcomb, W. W., Schafer, J. S., Chatenet, B., Lavenu, F., Kaufman, Y. J., Vande Castle, J., Setzer, A., Markham, B., Clark, D., Frouin, R., Halthore, R., Karneli, A., O'Neill, N. T., Pietras, C., Pinker, R. T., Voss, K., and Zibordi, G.: An emerging ground-based aerosol climatology: aerosol optical depth from AERONET, J. Geophys. Res., 106, 9807–9826, 2001.

Johnson, C. E., Mann, G. W., Bellouin, N., O'Connor, F. M., and Dalvi, M.: Comparison between UKCA-MODE and CLASSIC aerosol schemes in HadGEM3, Integrated Climate Programme Deliverable M3.2, Report CR-ICP-2007–2012 to DECC, Defra and MoD, available at: http://www.ukca.ac.uk/wiki/images/f/f8/ICP.pdf, (last access: 30 July 2012), 2010.

Jones, A., Roberts, D. L., Woodage, M. J., and Johnson, C. E.: Indirect sulphate aerosol forcing in a climate model with an interactive sulphur cycle, J. Geophys. Res., 106, 20293–20310, 2001.

Jones, A., Haywood, J. M., and Boucher, O.: Aerosol forcing, climate response and climate sensitivity in the Hadley Centre climate model, J. Geophys. Res., 112, D20211, doi:10.1029/2007JD008688, 2007.

Jones, G. S., Christidis, N., and Stott, P. A.: Detecting the influence of fossil fuel and bio-fuel black carbon aerosols on near surface temperature changes, Atmos. Chem. Phys., 11, 799–816, doi:10.5194/acp-11-799-2011, 2011.

Kirkby, J., Curtius, J., Almeida, J., Dunne, E., Duplissy, J., Ehrhart, S., Franchin, A., Gagné, S., Ickes, L., Kürten, Kupc, A., Metzger, A., Riccobono, F., Rondo, L., Schobesberger, S., Tsagkogeorgas, G., Wimmer, D., Amorim, A., Bianchi, F., Breitenlechner, M., David, A., Dommen, J., Downard, A., Ehn, M., Flagan, R. C., Haider, S., Hansel, A., Hauser, D., Jud, W., Junninen, H., Kreissl, F., Kvashin, A., Laaksonen, A., Lehtipalo, K., Lima, J., Lovejoy, E. R., Makhmutov, V., Mathot, S., Mikkilä, J., Minginette, P., Mogo, S., Nieminen, T., Onnela, A., Pereira, P., Petäjä, T., Schnitzhofer, R., Seinfeld, J. H., Sipilä, M., Stozhkov, Y., Stratmann, F., Tomé, A., Vanhanen, J., Viisanen, J., Vrtala, A., Wagner, P. E., Walther, H., Weingartner, E., Wex, H., Winkler, P. M., Carslaw, K. S., Worsnop, D. R., Baltensperger, U., and Kulmala, M.: Role of sulphuric acid, ammonia and galactic cosmic rays in atmospheric aerosol nucleation, Nature, 476, 429–433, doi:10.1038/nature10343, 2011.

Kokkola, H., Korhonen, H., Lehtinen, K. E. J., Makkonen, R., Asmi, A., Järvenoja, S., Anttila, T., Partanen, A.-I., Kulmala, M., Järvinen, H., Laaksonen, A., and Kerminen, V.-M.: SALSA – a Sectional Aerosol module for Large Scale Applications, Atmos. Chem. Phys., 8, 2469–2483, doi:10.5194/acp-8-2469-2008, 2008.

Lamarque, J.-F., Bond, T. C., Eyring, V., Granier, C., Heil, A., Klimont, Z., Lee, D., Liousse, C., Mieville, A., Owen, B., Schultz, M. G., Shindell, D., Smith, S. J., Stehfest, E., Van Aardenne, J., Cooper, O. R., Kainuma, M., Mahowald, N., McConnell, J. R., Naik, V., Riahi, K., and van Vuuren, D. P.: Historical (1850–2000) gridded anthropogenic and biomass burning emissions of reactive gases and aerosols: methodology and application, Atmos. Chem. Phys., 10, 7017–7039, doi:10.5194/acp-10-7017-2010, 2010.

Lauer, A., Hendricks, J., Ackermann, I., Schell, B., Hass, H., and Metzger, S.: Simulating aerosol microphysics with the ECHAM/MADE GCM – Part I: Model description and comparison with observations, Atmos. Chem. Phys., 5, 3251–3276, doi:10.5194/acp-5-3251-2005, 2005.

Lee, L. A., Carslaw, K. S., Pringle, K. J., Mann, G. W., and Spracklen, D. V.: Emulation of a complex global aerosol model to quantify sensitivity to uncertain parameters, Atmos. Chem. Phys., 11, 12253–12273, doi:10.5194/acp-11-12253-2011, 2011.

Liu, X., Penner, J. E., and Herzog, M.: Global modeling of aerosol dynamics: Model description, evaluation, and interactions between sulfate and nonsulfate aerosols, J. Geophys. Res., 110, D18206, doi:10.1029/2004JD005674, 2005.

Liu, X., Easter, R. C., Ghan, S. J., Zaveri, R., Rasch, P., Shi, X., Lamarque, J.-F., Gettelman, A., Morrison, H., Vitt, F., Conley, A., Park, S., Neale, R., Hannay, C., Ekman, A. M. L., Hess, P., Mahowald, N., Collins, W., Iacono, M. J., Bretherton, C. S., Flanner, M. G., and Mitchell, D.: Toward a minimal representation of aerosols in climate models: description and evaluation in the Community Atmosphere Model CAM5, Geosci. Model Dev., 5, 709–739, doi:10.5194/gmd-5-709-2012, 2012.

Manktelow, P. T., Carslaw, K. S., Mann, G. W., and Spracklen, D. V.: The impact of dust on sulfate aerosol, CN and CCN during an East Asian dust storm, Atmos. Chem. Phys., 10, 365–382, doi:10.5194/acp-10-365-2010, 2010.

Mann, G. W., Carslaw, K. S., Spracklen, D. V., Ridley, D. A., Manktelow, P. T., Chipperfield, M. P., Pickering, S. J., and Johnson, C. E.: Description and evaluation of GLOMAP-mode: a modal global aerosol microphysics model for the UKCA composition-climate model, Geosci. Model Dev., 3, 519–551, doi:10.5194/gmd-3-519-2010, 2010.

Martin, G. M., Ringer, M. A., Pope, V. D., Jones, A., Dearden, C., Hinton, T. J.: The physical properties of the atmosphere in the new Hadley Centre Global Environmental Model, HadGEM1. Part 1: Model description and global climatology, J. Clim., 19, 7, 1274–1301. doi:10.1175/JCLI3636.1, 2006.

The HadGEM2 Development Team: G. M. Martin, Bellouin, N., Collins, W. J., Culverwell, I. D., Halloran, P. R., Hardiman, S. C., Hinton, T. J., Jones, C. D., McDonald, R. E., McLaren, A. J., O'Connor, F. M., Roberts, M. J., Rodriguez, J. M., Woodward, S., Best, M. J., Brooks, M. E., Brown, A. R., Butchart, N., Dearden, C., Derbyshire, S. H., Dharssi, I., Doutriaux-Boucher, M., Edwards, J. M., Falloon, P. D., Gedney, N., Gray, L. J., Hewitt, H. T., Hobson, M., Huddleston, M. R., Hughes, J., Ineson, S., Ingram, W. J., James, P. M., Johns, T. C., Johnson, C. E., Jones, A., Jones, C. P., Joshi, M. M., Keen, A. B., Liddicoat, S., Lock, A. P., Maidens, A. V., Manners, J. C., Milton, S. F., Rae, J. G. L., Ridley, J. K., Sellar, A., Senior, C. A., Totterdell, I. J., Verhoef, A., Vidale, P. L., and Wiltshire, A.: The HadGEM2 family of Met Office Unified Model climate configurations, Geosci. Model Dev., 4, 723–757, doi:10.5194/gmd-4-723-2011, 2011.

Merikanto, J., Spracklen, D. V., Mann, G. W., Pickering, S. J., and Carslaw, K. S.: Impact of nucleation on global CCN, Atmos. Chem. Phys., 9, 8601–8616, doi:10.5194/acp-9-8601-2009, 2009.

Morcrette, J.-J., Boucher, O., Jones, L., Salmond, D., Bechtold, P., Beljaars, A., Benedetti, A., Bonet, A., Kaiser, J. W., Razinger, M., Schulz, M., Serrar, S., Simmons, A. J., Sofiev, M., Suttie, M., Tompkins, A. M., and Untch, A.: Aerosol analysis and forecast in the ECMWF Integrated Forecast System: forward modeling. J. Geophys. Res., 114, D06206, doi:10.1029/2008JD011235, 2009.

Myhre, G.: Consistency between satellite-derived and modeled estimates of the direct aerosol effect, Science, 325, 187–190, 2009.

O'Dowd, C. D., Lowe, J. A., and Smith, M. H.: Observations and modelling of aerosol growth in marine stratocumulus – case study, Atmos. Environ., 33, 3053–3062, 1999.

Penner, J. E., Xu, L., and Wang, M.: Satellite methods underestimate indirect climate forcing by aerosols, Proc. Nat. Acad. Sci., 108, 13404–13408, 2011.

Pringle, K. J., Carslaw, K. S., Spracklen, D. V., Mann, G. M., and Chipperfield, M. P.: The relationship between aerosol and cloud drop number concentrations in a global aerosol microphysics model, Atmos. Chem. Phys., 9, 4131–4144, doi:10.5194/acp-9-4131-2009, 2009.

Pringle, K. J., Tost, H., Message, S., Steil, B., Giannadaki, D., Nenes, A., Fountoukis, C., Stier, P., Vignati, E., and Lelieveld, J.: Description and evaluation of GMXe: a new aerosol submodel for global simulations (v1), Geosci. Model Dev., 3, 391–412, doi:10.5194/gmd-3-391-2010, 2010.

Quaas, J., Ming, Y., Menon, S., Takemura, T., Wang, M., Penner, J. E., Gettelman, A., Lohmann, U., Bellouin, N., Boucher, O., Sayer, A. M., Thomas, G. E., McComiskey, A., Feingold, G.,

Hoose, C., Kristjánsson, J. E., Liu, X., Balkanski, Y., Donner, L. J., Ginoux, P. A., Stier, P., Grandey, B., Feichter, J., Sednev, I., Bauer, S. E., Koch, D., Grainger, R. G., Kirkevåg, A., Iversen, T., Seland, Ø., Easter, R., Ghan, S. J., Rasch, P. J., Morrison, H., Lamarque, J.-F., Iacono, M. J., Kinne, S., and Schulz, M.: Aerosol indirect effects – general circulation model intercomparison and evaluation with satellite data, Atmos. Chem. Phys., 9, 8697–8717, doi:10.5194/acp-9-8697-2009, 2009.

Roberts, D. L. and Jones, A.: Climate sensitivity to black carbon aerosol from fossil fuel combustion, J. Geophys. Res., 109, D16202, doi:10.1029/2004JD004676, 2004.

Schmidt, A., Carslaw, K. S., Mann, G. W., Rap, A., Pringle, K. J., Spracklen, D. V., Wilson, M., and Forster, P. M.: Importance of tropospheric volcanic aerosol for indirect radiative forcing of climate, Atmos. Chem. Phys., 12, 7321–7339, doi:10.5194/acp-12-7321-2012, 2012.

Schulz, M., Textor, C., Kinne, S., Balkanski, Y., Bauer, S., Berntsen, T., Berglen, T., Boucher, O., Dentener, F., Guibert, S., Isaksen, I. S. A., Iversen, T., Koch, D., Kirkevåg, A., Liu, X., Montanaro, V., Myhre, G., Penner, J. E., Pitari, G., Reddy, S., Seland, Ø., Stier, P., and Takemura, T.: Radiative forcing by aerosols as derived from the AeroCom present-day and pre-industrial simulations, Atmos. Chem. Phys., 6, 5225–5246, doi:10.5194/acp-6-5225-2006, 2006.

Spracklen, D. V., Pringle, K. J., Carslaw, K. S., Chipperfield, M. P., and Mann, G. W.: A global off-line model of size-resolved aerosol microphysics: I. Model development and prediction of aerosol properties, Atmos. Chem. Phys., 5, 2227–2252, doi:10.5194/acp-5-2227-2005, 2005.

Spracklen, D. V., Carslaw, K. S., Kulmala, M., Kerminen, V.-M., Sihto, S.-L., Riipinen, I., Merikanto, J., Mann, G. W., Chipperfield, M. P., Wiedensohler, A., Birmili, W., and Lihavainen, H.: Contribution of particle formation to global cloud condensation nuclei concentrations, Geophys. Res. Lett., 35, L06808 doi:10.1029/2007GL033038, 2008.

Stier, P., Feichter, J., Kinne, S., Kloster, S., Vignati, E., Wilson, J., Ganzeveld, L., Tegen, I., Werner, M., Balkanski, Y., Schulz, M., Boucher, O., Minikin, A., and Petzold, A.: The aerosol-climate model ECHAM5-HAM, Atmos. Chem. Phys., 5, 1125–1156, doi:10.5194/acp-5-1125-2005, 2005.

Stier, P., Seinfeld, J. H., Kinne, S., and Boucher, O.: Aerosol absorption and radiative forcing, Atmos. Chem. Phys., 7, 5237–5261, doi:10.5194/acp-7-5237-2007, 2007.

Streets, D. G., Bond, T. C., Lee, T., and Jang C.: On the future of carbonaceous aerosol emissions, J. Geophys. Res., 109, D24212, doi:10.1029/2004JD004902, 2004.

Taylor, J. P. and McHaffie, A.: Measurements of cloud susceptibility, J. Atmos. Sci., 51, 10, 1298–1306, 1994.

Telford, P. J., Braesicke, P., Morgenstern, O., and Pyle, J. A.: Technical Note: Description and assessment of a nudged version of the new dynamics Unified Model, Atmos. Chem. Phys., 8, 1701–1712, doi:10.5194/acp-8-1701-2008, 2008.

van der Werf, G. R., Randerson, J. T., Giglio, L., Collatz, G. J., Kasibhatla, P. S., and Arellano Jr., A. F.: Interannual variability in global biomass burning emissions from 1997 to 2004, Atmos. Chem. Phys., 6, 3423–3441, doi:10.5194/acp-6-3423-2006, 2006.

Vignati, E., Wilson, J., and Stier, P.: M7: an efficient size-resolved aerosol microphysics module for large-scale aerosol transport models, J. Geophys. Res., 109, D22202, doi:10.1029/2003JD004485, 2004.

Wilson, D. R., Bushell, A. C., Kerr-Munslow, A. M., Price, J. D., and Morcrette, C. J.: PC2: a prognostic cloud fraction and condensation scheme. I: Scheme description, Q. J. Roy. Meteorol. Soc., 134, 2093–2107, doi:10.1002/qj.333, 2008.

Woodhouse, M. T., Carslaw, K. S., Mann, G. W., Vallina, S. M., Vogt, M., Halloran, P. R., and Boucher, O.: Low sensitivity of cloud condensation nuclei to changes in the sea-air flux of dimethyl-sulphide, Atmos. Chem. Phys., 10, 7545–7559, doi:10.5194/acp-10-7545-2010, 2010.

Woodhouse, M. T., Mann, G. W., Carslaw, K. S., and Boucher, O.: Sensitivity of cloud condensation nuclei to regional changes in dimethyl-sulphide emissions, Atmos. Chem. Phys., 13, 2723–2733, doi:10.5194/acp-13-2723-2013, 2013.

Yang, M., Huebert, B. J., Blomquist, B. W., Howell, S. G., Shank, L. M., McNaughton, C. S., Clarke, A. D., Hawkins, L. N., Russell, L. M., Covert, D. S., Coffman, D. J., Bates, T. S., Quinn, P. K., Zagorac, N., Bandy, A. R., de Szoeke, S. P., Zuidema, P. D., Tucker, S. C., Brewer, W. A., Benedict, K. B., and Collett, J. L.: Atmospheric sulfur cycling in the southeastern Pacific – longitudinal distribution, vertical profile, and diel variability observed during VOCALS-REx, Atmos. Chem. Phys., 11, 5079–5097, doi:10.5194/acp-11-5079-2011, 2011.